Factor-of-safety calculations in geomechanics

Author: Prof. Dr. habil. Heinz Konietzky
(TU Bergakademie Freiberg, Geotechnical Institute)

Editor: Prof. Dr.-Ing. habil. Heinz Konietzky Layout: Angela Griebsch
TU Bergakademie Freiberg, Institut für Geotechnik, Gustav-Zeuner-Straße 1, 09599 Freiberg • sekr_fm@ifgt.tu-freiberg.de

1 Introduction

Geo-Engineers have to proof stability and serviceability of geotechnical structures as demanded by EUROCODE and other regulations or recommendations. Serviceability is mainly related to deformations. Evaluation of stability / instability is mainly based on the balance between 'driving forces' and 'resisting forces'. Global instability is always connected with violation of serviceability, but - in reverse direction - violation of serviceability is not always connected to local or global failure.

It is important to distinguish between global failure and local failure. Global failure means the total collapse of a complete geotechnical structure (e.g. complete failure of a slope or total collapse of a tunnel). While local failure does not violate the stability of the overall structure, but concerns only very localized failure at critical points (e.g. single rockfall at the huge rockslope or local spalling at the surface of an opening).
Stability calculations can be performed by:

- Numerical calculations (no restrictions)
- Analytical limit equilibrium calculations (limited to simple constellations)
- Semi-analytical limit equilibrium calculations (some restrictions)
- Empirical rules, charts (restricted to equivalent conditions)

2 Factor-of-Safety (FOS) definitions

Stability can be quantified by the so-called Factor-of-Safety (FOS). Values below 1 characterize instability, values greater than 1 stability.

$$\begin{aligned} &FOS > 1 \quad \rightarrow \quad \text{stable} \\ &FOS = 1 \quad \rightarrow \quad \text{limit state} \\ &FOS < 1 \quad \rightarrow \quad \text{unstable} \end{aligned} \tag{2.1}$$

There are quite different FOS definitions in use, but most of them belong to one of the two principle definitions (Eq. (2.2a) and (2.2b)):

$$FOS = \frac{\text{failure load}}{\text{actual load}} \tag{2.2a}$$

Equation (2a) shows the definition for practical issues. For a given strength of a construction or structure, the FOS of the system can be determined for an applied stress state.

A different approach can be made for numerical modelling procedure, where strength parameters are step-by-step reduced until failure is observed (Eq. (2.2b)):

$$FOS = \frac{\text{actual strength parameter}}{\text{strength parameter, which leads to failure}} \tag{2.2b}$$

This very popular FOS definition (Eq. (2.2b)), also recommended by the EUROCODE, is based on the so-called shear strength reduction (SSR) technique. A good overview about about SSR is given by Diederichs et al. (2007). This method was first developed and applied on soil mechanics and is based on the Mohr-Coulomb strength criterion with cohesion c and friction angle φ (e.g. Duncan (1996) and Dawson et al. (2000)):

$$FOS = \frac{c}{c_{\text{failure}}} = \frac{\tan(\varphi)}{\tan(\varphi_{\text{failure}})} \tag{2.3}$$

Because rocks have significant lower tensile resistance than in compression, application in rock mechanics demands an extension by incorporation of tensile strength σ_T in the following form:

$$FOS = \frac{c}{c_{\text{failure}}} = \frac{\tan(\varphi)}{\tan(\varphi_{failure})} = \frac{\sigma_{\text{T}}}{\sigma_{\text{T,failure}}} \tag{2.4}$$

The shear strength reduction technique can also be applied to non-linear strength criteria, like the very popular Hoek-Brown criterion as shown by Chakraborti et al. (2012a, b).

3 Limit equilibrium versus numerical FOS calculation

If potential failure planes are clearly recognizable, e.g. weak interfaces between rock and building or already activated sliding plane, a limit equilibrium calculation can be performed. If the strength can be considered by the Mohr-Coulomb criterion and potential shear failure is assumed, the FOS can be determined by the following expression based on force equilibrium:

$$FOS = \frac{c_A + F_N \tan\varphi}{F_H} \tag{3.1}$$

where A represents the area of the considered potential failure plane, F_N represents the normal force acting on the failure plane and F_H is the force component parallel to the potential failure plane (shear force). If we compare the limit equilibrium procedure and the numerical one (FEM, FDM, FVM or DEM) to determine FOS, the following conclusions can be drawn (see also Table 3.1):

- Limit equilibrium methods are much faster than numerical calculations
- Model set-up is much easier for limit equilibrium methods
- Limit equilibrium tools are cheap, methods are popular and long-standing experience exist
- Numerical methods are more flexible in terms of geometry, initial and boundary con ditions as well as inclusion of support measures and HTM-coupling
- Limit equilibrium methods need the pre-specification of potential failure planes, numerical methods do not need that: any complex failure planes evolve naturally based on physical laws
- Numerical approach can be applied to any complex 3D situation, usually limit equilibrium methods are restricted to 2D problems

Tab. 3.1: Comparison between different methods to determine FOS

	Numerical solution	Limit equilibrium solution
Equilibrium	Satisfied everywhere	Satisfied only for specific objects (slices or block edges)
Stresses	Computed everywhere inside the model	Computed approximately on certain surfaces
Deformation	Always part of the solution	Not considered
Failure	Yield condition satisfied every-where; failure surfaces develop “automatically” as conditions dictate	Failure allowed only on certain pre-defined surfaces; no check on yield condition elsewhere
Kinematics	The “mechanisms” that develop satisfy kinematic constraints	Kinematics are not considered – mechanisms may not be feasible

For simple constellations limit equilibrium calculations and numerical calculations show nearly identical FOS values, like documented by Fig. 3.1 and 3.2 according to (Dawson et al., 1999). However, like exemplary shown in Fig. 3.3, 3.4 and 3.5 numerical simulation results can significantly deviate from classical limit equilibrium calculations in terms of FOS value including failure plane shape and location. This is mainly caused by the fact, that within limit equilibrium methods complex failure planes cannot develop.

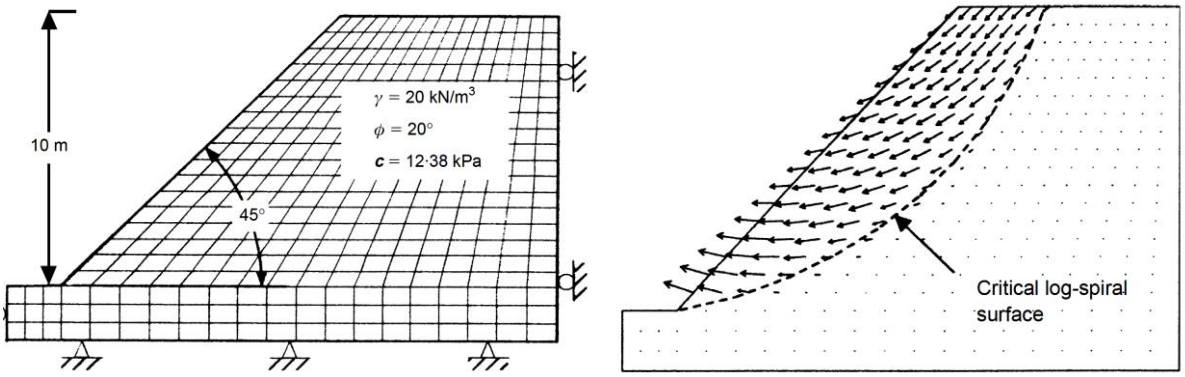

Fig. 3.1: Simple slope with corresponding parameters and failure surface (Dawson et al. 1999).

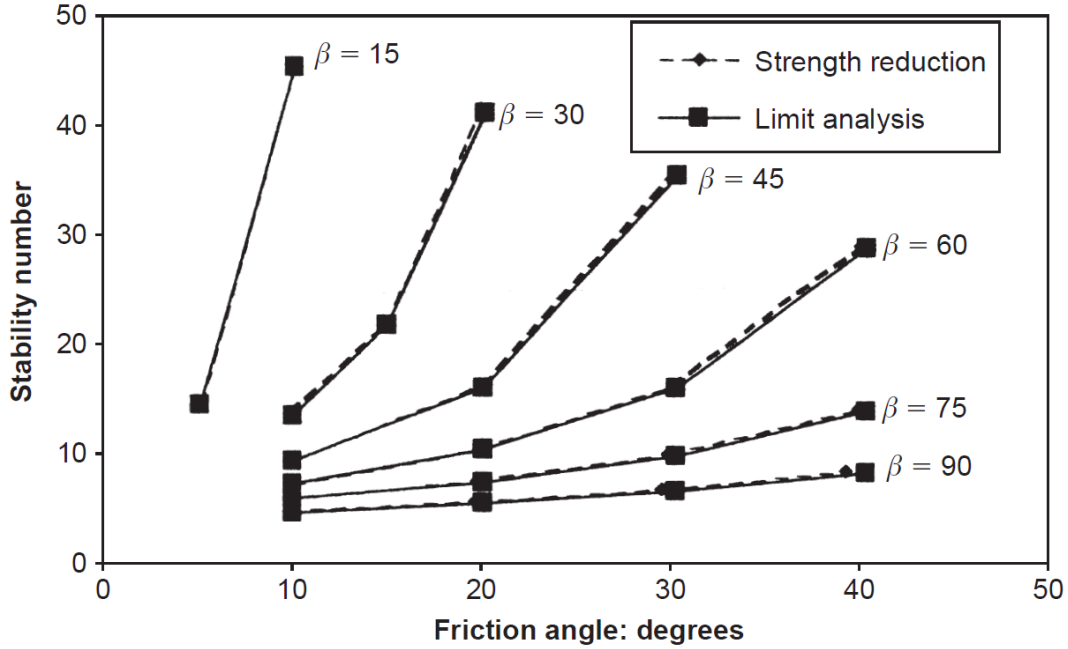

Fig. 3.2: Comparison between limit equilibrium und numerical calculation using shear strength reduction technique for a slope according to Fig. 3.1 (Dawson et al. 1999).

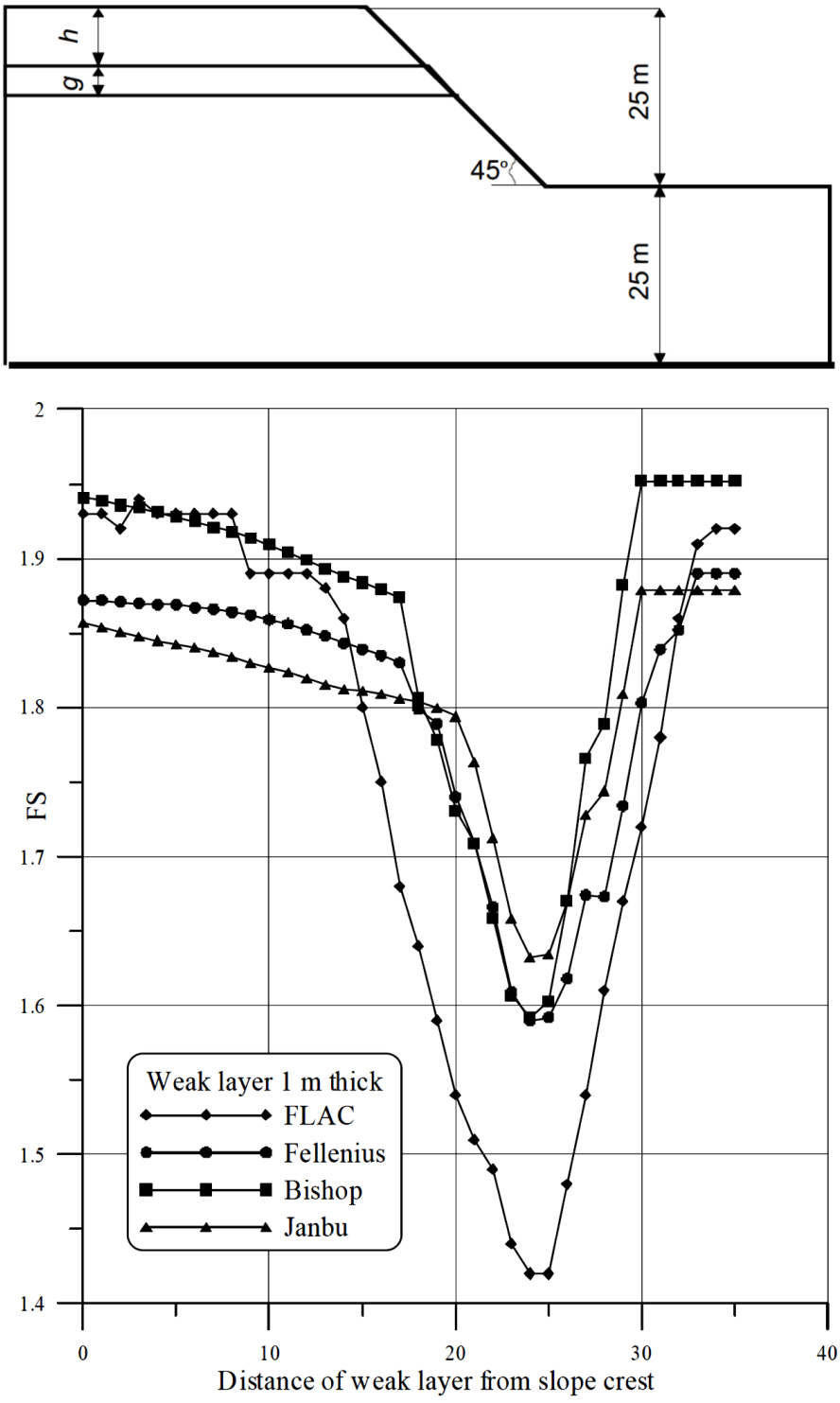

Fig. 3.3: FOS values for slope with thin weak layer g according to sketch above (Cala & Flisiak 2003)

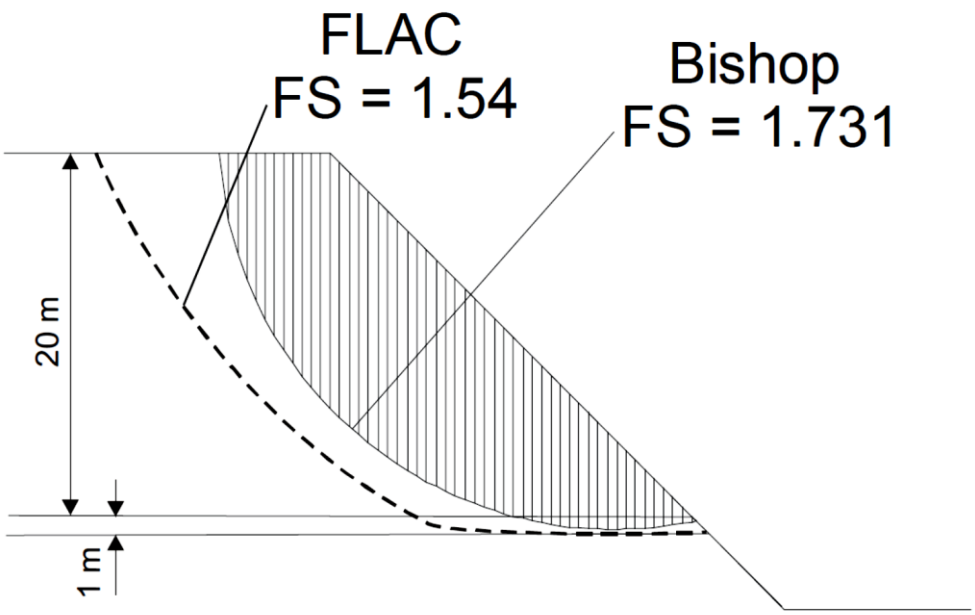

Fig. 3.4: Predicted failure planes for slope model according to Fig. 3 (Cala & Flisiak 2003)

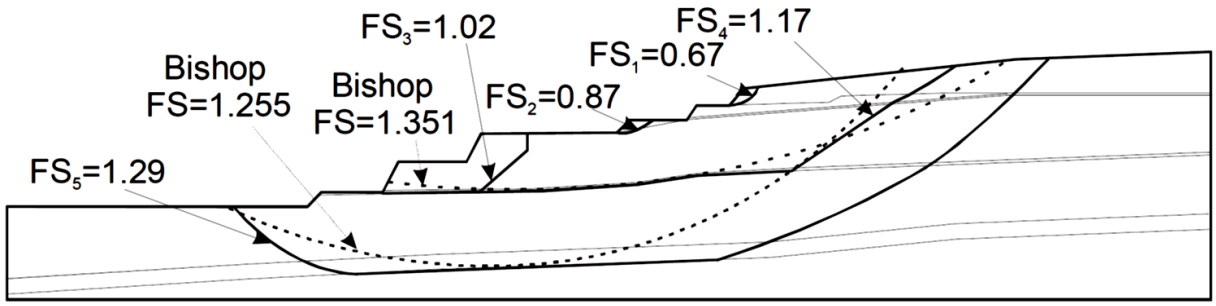

Fig. 3.5: Predicted failure planes and FOS values for complex slope using SSR and limit equilibrium calculations (Cala & Flisiak 2003).

Especially for slopes, it should be noticed, that FOS values determined under 2D conditions are often very conservative. In most cases 3D calculations instead deliver much higher FOS values (Cala & Flisiak 2006).

4 Assessment and illustration of local FOS

A simplified approach to detect areas of potential local shear failure consists of the following steps:

- run a numerical model under the assumption of pure elasticity or with elasto-plastic parameters
- compare the stress state with a chosen failure criterion
- define a measure how far the actual elastic stress state is away from the failure envelope

In the following two different definitions are explained. The first approach compares two line segments from the center of Mohr's stress circle perpendicular to the linear failure envelope of the Mohr-Coulomb failure criterion (Fig. 4.1 and Eq. 4.1). The second approach (Fig. 4.2 and Eq. 4.2) compares the actual radius of Mohr's stress circle with a hypothetical circle which touches the failure envelope (limit state). The second definition can also be applied for non-linear failure envelopes like the Hoek-Brown failure criterion.

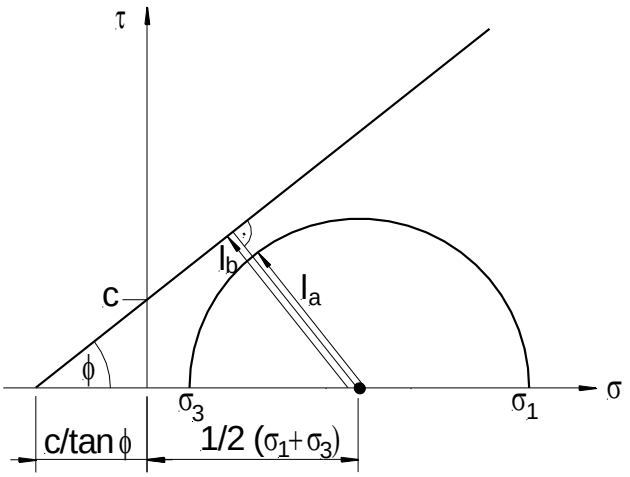

Fig. 4.1: Definition of FOS based on Mohr's stress circle and Mohr-Coulomb failure envelope.

$$FOS = \frac{L_b}{L_a} = \frac{\sin\varphi \cdot \left(\dfrac{c}{\tan\varphi} + \dfrac{1}{2}\left(\sigma_1 + \sigma_3\right) \right)}{\dfrac{1}{2}\left(\sigma_1 - \sigma_3\right)} \tag{4.1}$$

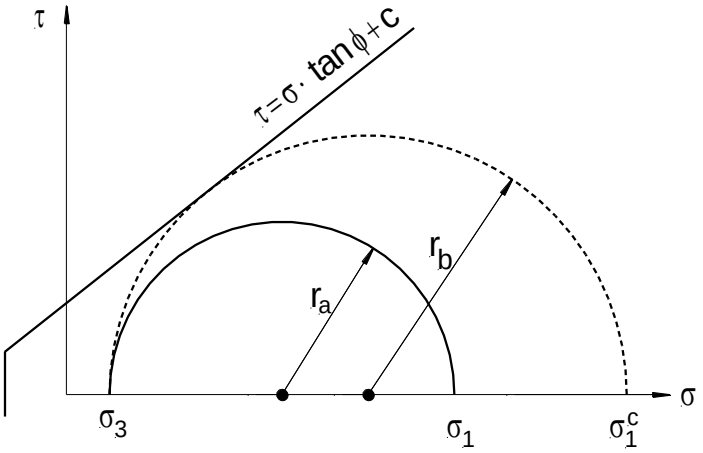

Fig. 4.2: Definition of FOS based on Mohr's stress circle and Mohr-Coulomb failure envelope.

$$FOS = \frac{r_b}{r_a} = \frac{\sigma_1^c - \sigma_3}{\sigma_1 - \sigma_3} \tag{4.2}$$

$$\sigma_1^c = \kappa \cdot \sigma_3 - 2c\sqrt{\kappa} \quad \text{with} \quad \kappa = \frac{1+\sin\varphi}{1-\sin\varphi} \quad \text{for Mohr-Coulomb criterion} \tag{4.3}$$

$$\sigma_1^c = \sigma_3 - \sqrt{-m\sigma_c\,\sigma_3 + s\sigma_c^2} \qquad \text{for Hoek-Brown criterion} \qquad (4.4)$$

m, σ_c, *s*, *c* and φ are material parameter.

Fig. 4.3 illustrates a slope with calculated FOS values according to Eq. 4.2 and specification of certain strength parameters. In a similar way a FOS value against tensile failure can be determined and illustrated by comparison between minimum principal stress and tensile strength.
More information about the safety of geotechnical structures can be obtained by detailed evaluation of the stress state in comparison to the failure envelope and the plasticity state.

Exemplary, Fig. 4.4 shows part of a numerical pillar model (underground room and pillar mining) which consists of several types of rock with different strength parameters. The right hand side of Fig. 4.4 shows the plasticity state for a certain value of strength reduction and Fig. 4.5 shows the stress values of all elements in the principal stress space (σ_1 vs σ_3) together with failure envelopes for the three different types of rock under consideration. As Fig. 4.5 shows, that stresses inside the ‘red’ material are far away from the failure envelope (high FOS), the stresses inside the ‘green’ material are still away from the failure envelope, but stresses inside the ‘light blue’ material are mainly located at the failure envelope (limit state).

Fig. 4.6 illustrates how different strength reduction values influence the plasticity behavior (example from underground room and pillar mining).

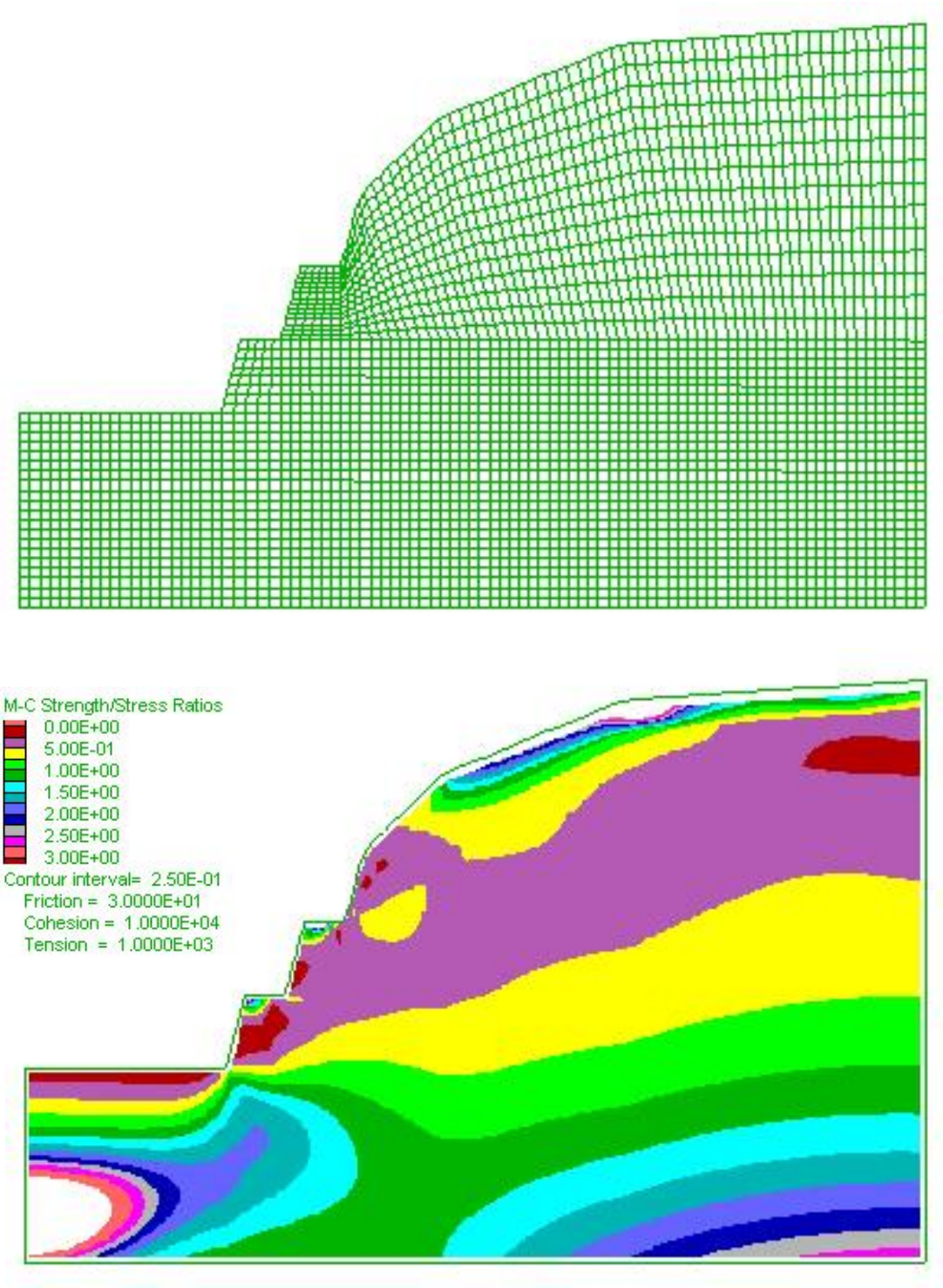

Fig. 4.3: Slope model (above) with corresponding isolines for FOS values (below) according to Eq. 4.2 under assumption of Mohr-Coulomb constitutive law and the following strength parameters: cohesion 1e4 Pa, friction angle 30°, tensile strength 1e3 Pa (FOS values > 3 are omitted).

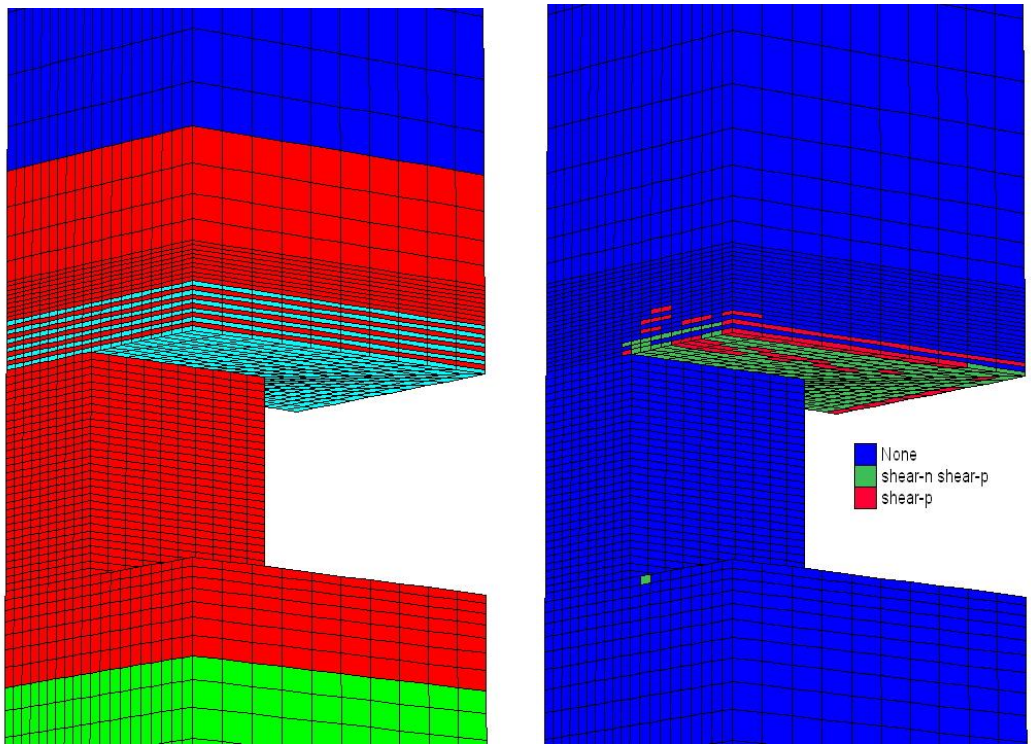

Fig. 4.4: Numerical pillar model (left: different colors represent different types of rock; right: plasticity state).

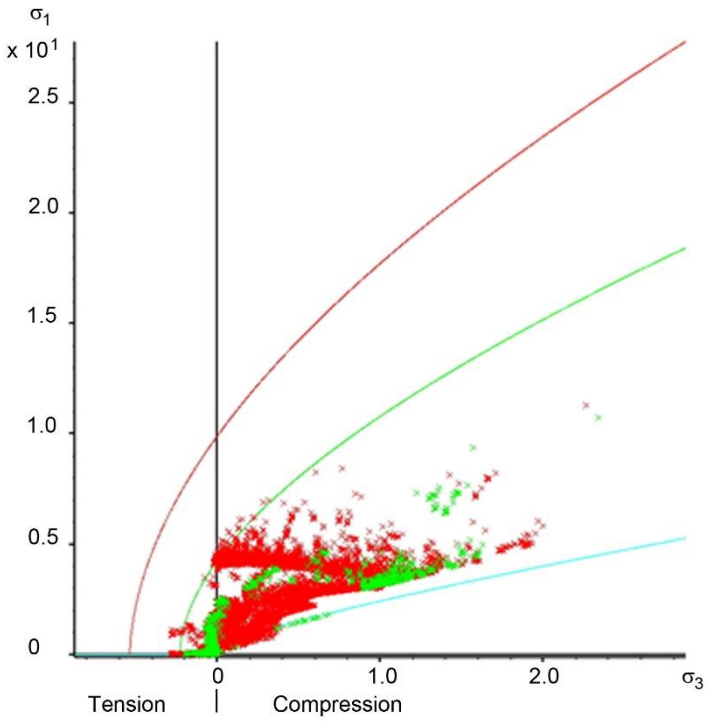

Fig. 4.5: Principal stress diagram with failure envelopes and stress values for 3 rock types obtained from the model according to Fig. 4.4.

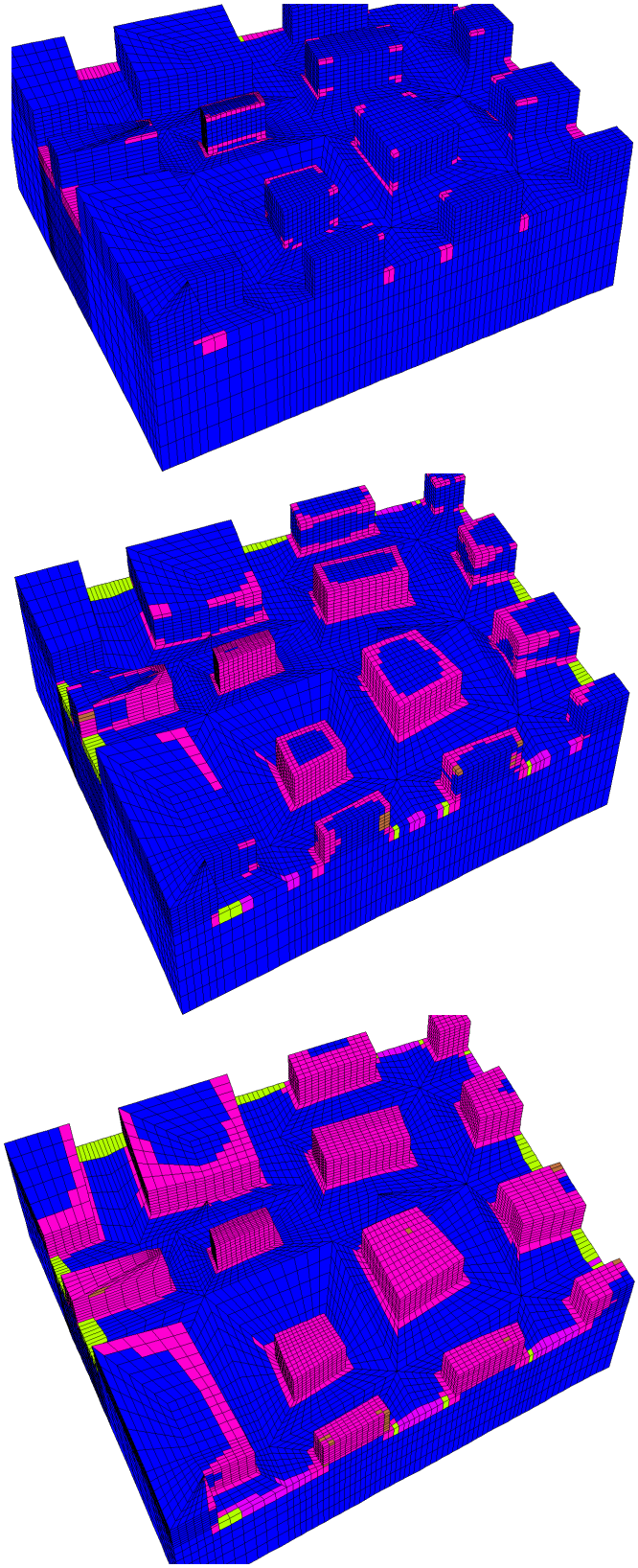

Fig. 4.6: Plasticity state for model with different applied strength reduction values (from top to bottom: 1.0, 1.5 and 2.0; Walter & Konietzky 2008).

5 FOS of arced slopes

Note, that FOS of arc shaped slopes deviate from “common” (not arced, straight) slopes as documented in Fig. 5.1. Also boundary conditions (SS, RS and RR see Fig. 5.1) have influence.

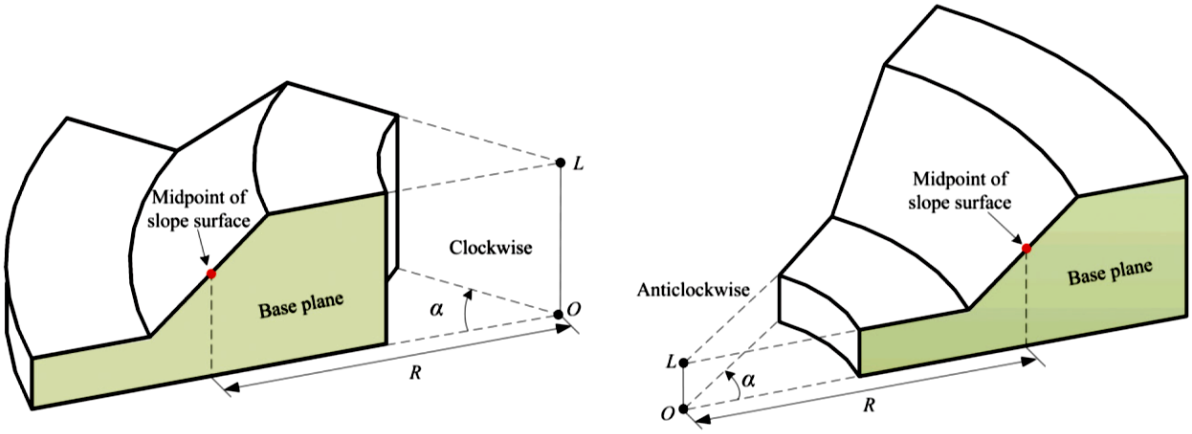

(a) Convex-turning arc (b) Concave-turning arc

Table 6. Stability of 3D slopes with different turning arcs for the three examples under different boundary conditions.

	Turning arc		Smooth–smooth (SS)		Rough–smooth (RS)		Rough–rough (RR)	
Example	Curvature	Angle (°)	FoS	DF (%)	FoS	DF (%)	FoS	DF (%)
1	Convex	45	1.62	−2.99	1.69	−6.63	1.93	−6.31
		90	1.62	−2.99	1.63	−4.68	1.69	−6.63
		180	1.62	−2.99	1.62	−3.57	1.63	−4.68
	Common	$W = 45°\times\pi R/180$	1.67	—	1.81	—	2.06	—
		$W = 90°\times\pi R/180$	1.67	—	1.71	—	1.81	—
		$W = 180°\times\pi R/180$	1.67	—	1.68	—	1.71	—
	Concave	45	1.93	15.57	2.00	10.50	2.20	6.80
		90	1.93	15.57	1.94	13.45	2.00	10.50
		180	1.93	15.57	1.93	14.88	1.94	13.45
2	Convex	45	1.87	2.75	1.96	−0.51	2.20	−1.79
		90	1.87	2.75	1.89	1.07	1.96	−0.51
		180	1.87	2.75	1.88	2.73	1.89	1.07
	Common	$W = 45°\times\pi R/180$	1.82	—	1.97	—	2.24	—
		$W = 90°\times\pi R/180$	1.82	—	1.87	—	1.97	—
		$W = 180°\times\pi R/180$	1.82	—	1.83	—	1.87	—
	Concave	45	2.10	15.38	2.16	9.64	2.37	5.80
		90	2.10	15.38	2.12	13.37	2.16	9.64
		180	2.10	15.38	2.10	14.75	2.12	13.37
3	Convex	45	2.20	4.76	2.25	1.35	2.41	0
		90	2.20	4.76	2.21	3.26	2.25	1.35
		180	2.20	4.76	2.20	3.77	2.21	3.26
	Common	$W = 45°\times\pi R/180$	2.10	—	2.22	—	2.41	—
		$W = 90°\times\pi R/180$	2.10	—	2.15	—	2.22	—
		$W = 180°\times\pi R/180$	2.10	—	2.12	—	2.15	—
	Concave	45	2.32	10.48	2.37	6.76	2.53	4.98
		90	2.32	10.48	2.34	8.84	2.37	6.76
		180	2.32	10.48	2.32	9.43	2.34	8.84

Note: Turning radius, R, is 10, 11, and 36 m for examples 1, 2, and 3, respectively (see Fig. 10). Width of the common slope, W, is equal to the midline width of the turning arc.

Fig. 5.1: FOS values of arc shaped slopes (Zhang et al., 2013) incl. difference to plane slope

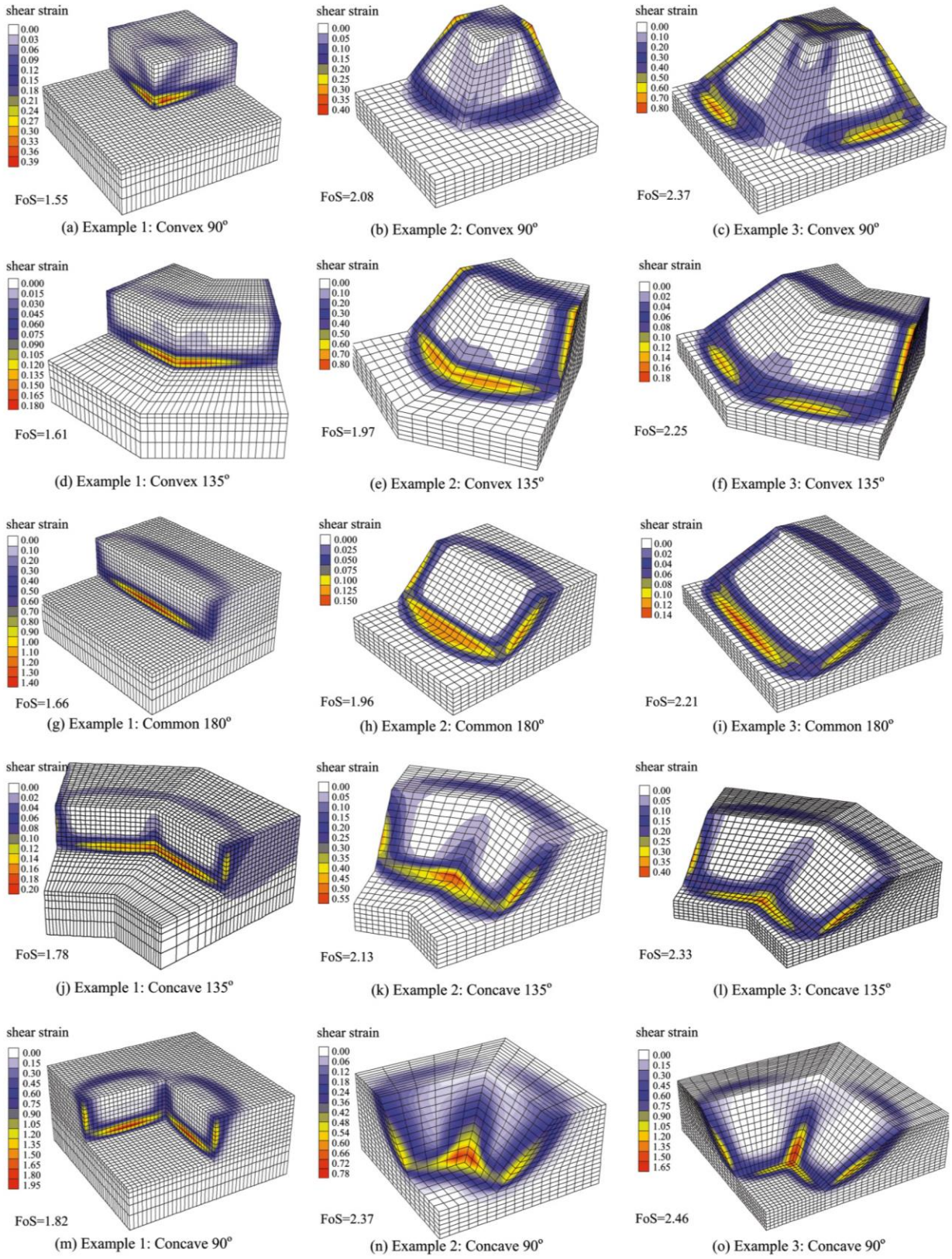

Fig. 5.2: FOS values and accumulated shear strain for slope models given in Fig. 4.7 (Zhang et al., 2013) .

Convex or concave shaped slopes can have either lower of higher FOS compared with common slopes (see also Fig. 5.2). The deviation is also influenced by the steepness. Deviation can be - depending how strong the geometry deviates – quite significant. Therefore, 2-dimensional approaches should be use with caution. See also Zhu et al. (2020).

Tianwen et al. (2017) investigated the slope stability based on Bishop's semi-analytical approach, but extending to 3D. They found a general increase in stability compared to a common slope, as documented by Fig. 5.3 .

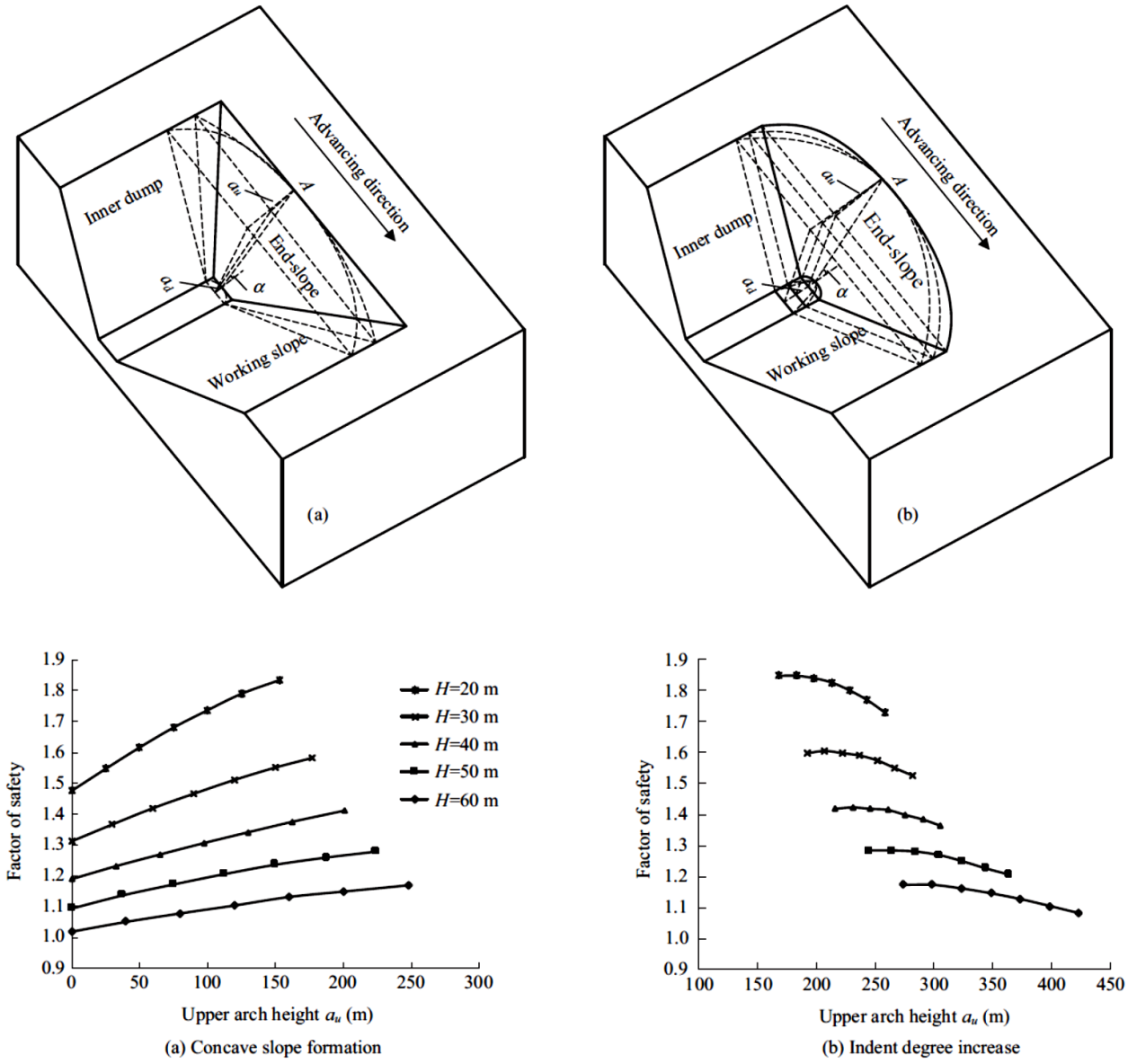

Fig. 5.3: FOS for concave shaped slopes with different curvature and height (Tianwen et al., 2017)

6 Utilization degree or factor

Another possibility to characterize the safety or stability of a structure is the determination of the so-called utilization degree. The utilization degree determines the stress state at the countour area or near-field of a structure (tunnel, cavern etc.) und compares this stress state with crtitical (failure) value. The utilization degree can be determined for selected points or as average value for a certain region / area (pillar, wall etc.).

The utilization degree η in general is defined as follows (in fact it can be considered as the inverse of the factor-of-safety):

$$\eta = \frac{existing\,stress}{failure\,stress} \tag{6.1}$$

A very common application of the uitilization degree is the characterization of the safety status of gas caverns (see for instance Rokahr & Staudtmeister, 1993 or Zapf, 2014) They use the second deviatoric stress invariant as stress criterion:

$$\eta = \frac{\sqrt{2 \cdot J^{D}_{2,actual}}}{\sqrt{2 \cdot J^{D}_{2,failure}(I_1)}} \tag{6.2}$$

For the denominator of Eq. 6.1 often the short term strength of the rock material is used.

Habibi (2019) provides an overview about evaluation criteria for salt caverns used worldwide.

Exemplary, Fig. 6.1 shows the utilization degree for a single cavern under the assumption of a certain stress state inside the rock mass, a certain gas pressure, a certain temperature and a certain failure stress state – calculated according to Eq. 6.2. Note, that the deviatoric failure stress state is a function of the current stress level, normally determined as function of the first stress invariant I_1.

In case of a cavern field Rokahr & Staudmeister (1993) proposed the use of an integral utilization degree for evaluation of the pillars between the caverns according to the follwing formula (see also Fig. 6.2):

$$\eta_{total} = \frac{\sum_{i=1}^{n} \left(\eta_i \cdot dV_i \right)}{V_{total}} \tag{6.3}$$

Eq. 6.3 provides an average utilization degree for a certain area (for instance a considered cross section) or a certain volume.

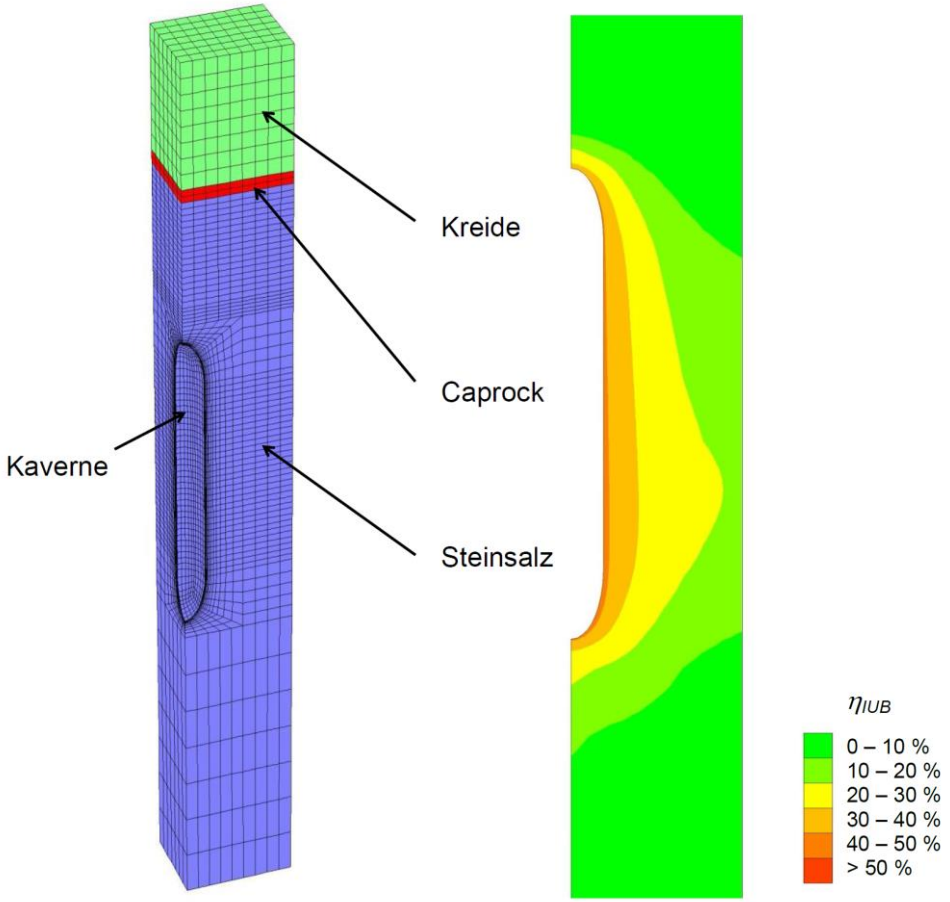

Fig. 6.1: Example: utilization degree for a single gas cavern under a certain pressure and temperature regime (Zapf, 2014).

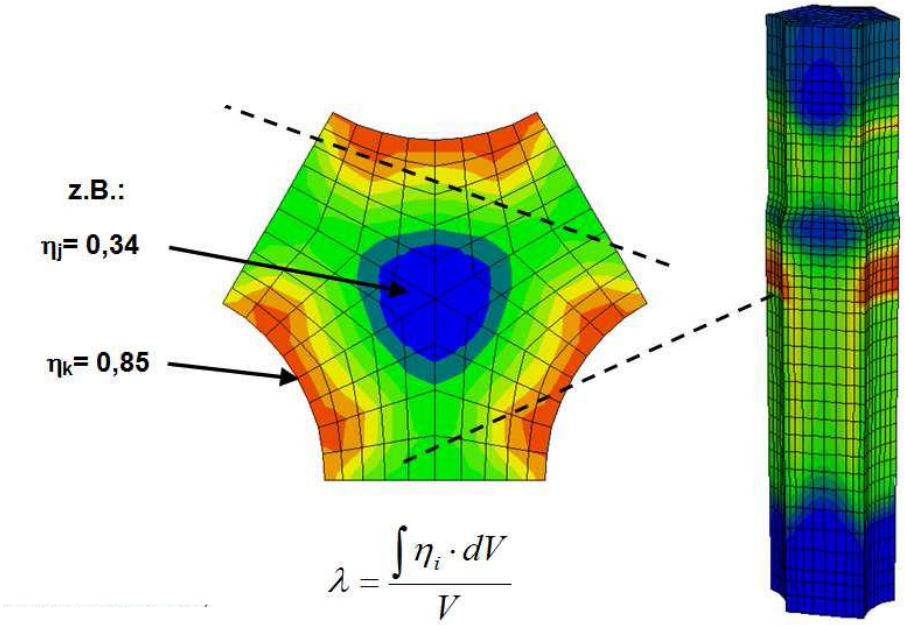

Fig. 6.2: Example: integral utilization degree for a pillar between gas caverns inside a regular cavern field according to the procedure proposed by Rokahr & Staudtmeister (1993).

7 Factor-of-safety and failure probability

The classical FOS calculation as discussed above is based on a fixed basic strength data set and the subsequent reduction of the strength parameters until failure is observed. The problem, however, is that we have uncertainty in strength parameters, the stress field and other influencing factors (e.g. geometry, support measures, temperature etc.). Therefore, a probabilistic approach is more appropriate. Wiles (2006) has shown, how FOS and probability of failure can be correlated under certain simplified assumptions (generalized normal distribution of parameters, Mohr-Coulomb strength criterion) and came up with the following expression:

$$FOS = \frac{1}{1 - CoV \cdot N^{-1}(P)} \qquad (7.1)$$

where:

CoV	=	coefficient of variation (standard deviation / mean value)
$N^{-1}(P)$	=	Inverse probability P assuming normal distribution

The uncertainty in parameters in geoengineering praxis - expressed as coefficient of variation - is typically between 20% and 40%. Table 7.1 relates FOS and failure probability according to Eq. (7.1).

Tab. 7.1: Relation between FOS, CoV and failure probability

FOS	**Coefficient of Variation CoV**	**Probability of failure P**
1.5	20 %	5 %
2.0	20 %	0.7 %
2.5	20 %	0.2 %
3.0	20 %	0.05 %
FOS	**Coefficient of Variation**	**Probability of failure**
1.5	30 %	13 %
2.0	30 %	5 %
2.5	30 %	2 %
3.0	30 %	1 %
FOS	**Coefficient of Variation**	**Probability of failure**
1.5	40 %	20 %
2.0	40 %	10 %
2.5	40 %	7 %
3.0	40 %	5 %

Please note, that a failure probability of about 5% is generally accepted for many geotechnical projects.

8 Literature

Cala, M. & Flisiak, J. (2003). Complex geology slope stability analysis by shear strength reduction. In: FLAC and numerical modeling in geomechanics : Proc. of the 3rd International FLAC Symposium.Ontario, Publisher: A.A. Balkema. 99-102

Cala, M., Flisiak, J. & Tajdus, A. (2006). Slope stability analysis with FLAC in 2D and 3D. In: Hart, R.D. & Varona, P. (Eds.), Proc. of the 4th International FLAC Symposium on Numerical Modeling in the Geomechanics, Madrid, Paper 01–02

Chakraborti, D., Konietzky, H. & Walter, K. (2012a). A Comparative Study of Different Approaches for Factor of Safety Calculations by Shear Strength Reduction Technique for Non-linear Hoek-Brown Failure Criterion. Geotech. Geol. Eng., 30(4): 925-934

Chakraborti, S., Konietzky, H. & Otparlik, K. (2012b). Global and local approach of numerical shear strength reduction techniques for materials characterized by Hoek-Brown criterion: a comparative study. In: Proc. EUROCK, Stockholm, Sweden (2012), (124): 1-13.

Dawson, E.M., Roth, W.H. & Drescher, A. (1999). Slope stability analysis by strength reduction. Geotechnique, 49(6): 835-840

Diederichs, M.S. et al. (2007). Shear strength reduction (SSR) approach for slope stability analysis. In: Proc. of 1st Canada–U.S. Rock Mechanics Symposium, Vancouver (May 2007): 319–327

Duncan, J.M. (1996). State of the art: limit equilibrium and finite-element analysis of slopes. J. Geotech. Eng., 122(7): 577-596

Habibi, R. (2019): An investigation into design concepts, design methods and stability criteria of salt caverns, Oil & Gas Science and Technology - Revue d'IFP Energies nouvelles, Institut Français du Pétrole, 74

Rokahr, R. & Staudtmeister, K. (1993): Assessment of the stability of a gas cavern in rock salt during sudden drop in internal pressure to atmospheric level, Proc. Eurock'93, 693-700

Tianwen, Z. et al. (2017): 3D stability analysis method of concave slope based on the Bishop method, Inj. J. Rock Mech. Min. Sci., 27: 365-370

Walter, K. & Konietzky, H. (2008). Room pillar dimensioning for gypsum and anhydrite mines in Germany. In: Proc. of the International Conference on Advances in Mining and Tunneling, Hanoi, Vietnam (2008): 349-362

Wiles, T.D. (2006): Reliability of numerical modelling predictions, iJRMMSci, 43: 454-472

Zapf, D. (2014): Dimensionierung von Gasspeicherkavernen im Salzstockrandbereich, PhD thesis, University Hannover

Zhang, Y. et al. (2013): Effects of geoemtries on three-dimensional slope stability, Can. Geotech. J., 50: 233-249

Zhou, Y. et al. (2020): Topographic effects on three-dimensional slope stability for fluctuating water conditions using numerical analysis, water, 12: 615